AAS 15-523

MULTI-OBJECTIVE HYBRID OPTIMAL CONTROL FOR MULTIPLE-FLYBY INTERPLANETARY MISSION DESIGN USING CHEMICAL PROPULSION

Jacob A. Englander[*], **Matthew A. Vavrina**[†]

Preliminary design of high-thrust interplanetary missions is a highly complex process. The mission designer must choose discrete parameters such as the number of flybys and the bodies at which those flybys are performed. For some missions, such as surveys of small bodies, the mission designer also contributes to target selection. In addition, real-valued decision variables, such as launch epoch, flight times, maneuver and flyby epochs, and flyby altitudes must be chosen. There are often many thousands of possible trajectories to be evaluated. The customer who commissions a trajectory design is not usually interested in a point solution, but rather the exploration of the trade space of trajectories between several different objective functions. This can be a very expensive process in terms of the number of human analyst hours required. An automated approach is therefore very desirable. This work presents such an approach by posing the impulsive mission design problem as a multi-objective hybrid optimal control problem. The method is demonstrated on several real-world problems.

INTRODUCTION

Preliminary design of high-thrust interplanetary missions is a highly complex process. The mission designer must choose discrete parameters such as the number of flybys and the bodies at which those flybys are performed. For some missions, such as surveys of small bodies, the mission designer also contributes to target selection. In addition, real-valued decision variables, such as launch epoch, flight times, maneuver and flyby epochs, and flyby altitudes must be chosen. There are often many thousands of possible trajectories to be evaluated. The customer who commissions a trajectory design is not usually interested in a point solution, but rather the exploration of the trade space of trajectories between several different objective functions. This can be a very expensive process in terms of the number of human analyst hours required, and so an automated approach is very desirable.

Two assumptions are frequently made to simplify the modeling of an interplanetary high-thrust trajectory [1] during the preliminary design phase. The first assumption is that because the available thrust is high, any maneuvers performed by the spacecraft can be modeled as discrete changes in velocity. This assumption removes the need to integrate the equations of motion governing the motion of a spacecraft under thrust and allows the change in velocity to be modeled as an impulse and the expenditure of propellant to be modeled using the time-independent solution to Tsiolkovsky's rocket equation [1]. The second assumption is that the spacecraft moves primarily under the influence of the central body, *i.e.* the sun, and all other perturbing forces may be neglected in preliminary design. The path of the spacecraft may then be modeled as a series of conic sections. When a spacecraft performs a close approach to a planet, the central body switches from the sun to that planet and the trajectory is modeled as a hyperbola with respect to the planet. This is known

[*] Aerospace Engineer, Navigation and Mission Design Branch, NASA Goddard Space Flight Center, Greenbelt, MD, 20771, USA, Member AIAA

[†] Senior Systems Engineer, a.i. solutions, Inc., 10001 Derekwood Ln. Suite 215, Lanham, MD, 20706, USA

as the method of patched conics [1]. The impulsive and patched-conic assumptions significantly simplify the preliminary design problem.

Many researchers have addressed the problem of finding the optimal high-thrust mission for a fixed destination and flyby sequence. Of particular relevance to this work are methods which employ stochastic global search methods such as genetic algorithms, differential evolution, particle swarm optimization, monotonic basin hopping (MBH), ant colony optimization, and inflationary differential evolution [2, 3, 4, 5, 6, 7]. These techniques, when coupled with an appropriate transcription [2, 4], are capable of finding globally optimal solutions to the fixed-sequence interplanetary mission design problem without requiring any *a priori* knowledge of the solution. However the works cited above only address the design problem for a fixed flyby sequence and destination and are therefore not sufficient to solve the full mission design problem.

The traditional method to search over a wide space of possible destinations and/or flyby sequences is to grid over candidate sequences, launch epochs, and planet-to-planet flight times and represent the trajectory between each pair of bodies with either a Lambert arc [8] or an arc which includes a deep-space maneuver (DSM) [9]. Alternatively, one can design the mission one body-to-body phase at a time using a graphical approach involving Pork Chop Contour and orbital resonance plots [10]. However as the size of the design space increases, *i.e.* as flybys, destinations, or DSMs are added, grid searches become more and more expensive. Other techniques which may be more efficient than a grid search also exist. Gad and Abdelkhalik [11, 12] solve the multiple-flyby problem using a genetic algorithm (GA) with mixed-integer programming. Another method, by Vasile and Campagnola [13], uses a set of successive deterministic algorithms to find candidate low-thrust, multiple flyby trajectories.

Another approach is to formulate the interplanetary design problem as a hybrid optimal control problem (HOCP). A HOCP is an optimization problem that is composed of two separable sub-problems, one with discrete variables and the other with continuous variables [14, 15]. For interplanetary design, the first problem is to choose the discrete parameters that define the mission, such as number of flybys, choice of flyby bodies, and, for some types of missions, the destination. The second problem is to find the time history of control variables, such as launch date, flight times, thrust magnitude and direction, flyby altitudes, and encounter velocity vectors that characterize the optimal trajectory for each set of discrete parameters. A HOCP can be solved using two nested optimization loops. The "outer-loop" solves the integer programming problem defining the discrete parameters. Each candidate solution to the "outer-loop" problem defines an "inner-loop" trajectory optimization problem. This approach was demonstrated first by Chilan, Wall, and Conway [16] for trajectories without flybys and then by Englander, Conway, and Williams for trajectories that include flybys and either impulsive chemical propulsion [17] or low-thrust electric propulsion [18]. All of these methods used a GA to solve the outer-loop problem and a variety of stochastic global search algorithms to solve the inner-loop problem.

However, all of the methods above find only a single "optimal" trajectory, that is, optimal according to a single objective function. Preliminary mission design requires the exploration of a multi-objective trade space. The designer must find not a single solution but instead the Pareto front, surface, or hyper-surface (depending on the number of objectives) between several objective functions. Several researchers have addressed such problems in the past for problems with a fixed flyby sequence and fixed destination. Coverstone-Carroll, Hartmann, and Mason [19] used a multi-objective GA with an indirect trajectory optimizer. Vavrina and Howell [20] also used a multi-objective GA hybridized with a direct trajectory optimization method. Both research groups found non-dominated fronts of delivered mass versus flight time. In addition, Vasile and Zuiani [21] demonstrated a multi-objective algorithm for finding the non-dominated front between flight time and Δv for impulsive-thrust missions with fixed destination and flyby sequence. Most recently, Izzo *et al.* developed a multi-objective algorithm for finding the optimal Jovian capture trajectory given a fixed sequence of moon flybys [22].

In this work we present a new framework for multi-objective optimization of low-thrust interplanetary trajectories where the flyby sequence, and sometimes the destinations themselves, are not known *a priori*. The approach presented here is an extension of the HOCP technique for low-thrust trajectory and sytems design previously introduced by these authors [23, 24]. The mission design problem is formulated as a HOCP

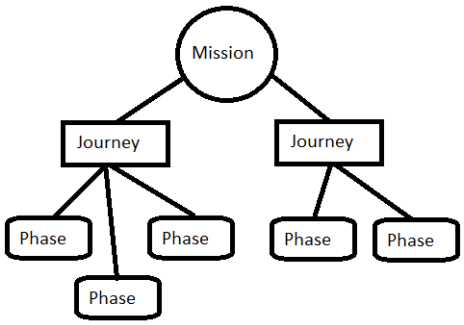

Figure 1: Anatomy of a Mission

where the outer-loop chooses the number of flybys, the identity of the flyby bodies, and, when appropriate, the destination. The outer-loop is based on the "null-gene" transcription presented by Englander, Conway, and Williams [17], a "cap and optimize" approach for varying the flight time and launch date, and the Non-Dominated Sorting Genetic Algorithm II (NSGA-II) multi-objective GA developed by Deb [25]. The inner-loop is based on a modified version of the multiple gravity assist with deep-space maneuver (MGADSM) transcription described by Vinkó and Izzo [4] which is constructed to interface with the stochastic global search algorithm MBH [26, 27, 7].

The proposed technique is demonstrated on several example problems, including a notional mission to Jupiter in the 2020s and a mission to deliver a kinetic impactor to and then inspect a near-Earth object.

PHYSICAL MODELING

Mission Architecture

Three layers of event types are defined in this work: *missions*, *journeys*, and *phases*. A *mission* is a top-level container that encompasses all of the events including departures, arrivals, impulsive maneuvers, coast arcs, and flybys. A *journey* is a set of events within a mission that begin and end target of interest, *i.e.* not just a body that is being used for a propulsive flyby. For example, the interplanetary cruise portion of the Cassini mission was composed of a single journey that began at Earth and ended at Saturn. JAXA's Hayabusa mission, which rendezvoused and took samples from near Earth asteroid Itokawa, had two journeys - one from Earth to Itokawa, and one from Itokawa to Earth. NASA's upcoming OSIRIS-REx mission is also composed of two journeys, one from Earth to Bennu and one from Bennu to Earth. Each journey is composed of one or more *phases*. Like a journey, a phase begins at a planet and ends at a planet, but unlike the end points of a journey, the end points of a phase may represent a flyby of a body that is being used only to modify the trajectory of the spacecraft, *i.e.* a propulsive flyby. For example, the first journey of the OSIRIS-REx mission may be considered to be a two-phase journey because it included a flyby of Earth. The number of journeys in a mission is fixed *a priori* but the number of phases is not, and in the context of this work both the number of phases and the identity of the flyby planets in each phase may be chosen by the optimizer. Figure 1 is a block diagram of a mission using the journey/phase nomenclature.

The Multiple Gravity Assist with one Deep-Space Maneuver Transcription

The transcription used in this work is the MGADSM developed first by Vasile and De Pascale [2], and then by Vinkó and Izzo [4]. Planetary flybys in MGADSM are modeled via a patched-conic approximation and a DSM is allowed at any point along each planet-to-planet phase. If a DSM is not required, the inner-loop solver will drive its magnitude to zero. The MGADSM model is inexpensive to evaluate and, coupled with a suitable inner-loop optimizer, allows rapid optimization of trajectories in low fidelity suitable for preliminary design.

In the first phase of an MGADSM, the spacecraft is assumed to start with the same state vector as the planet

from which it launches. An impulse, with magnitude bounded by the maximum heliocentric velocity that the launch vehicle can impart to the spacecraft, is applied in a chosen direction. This impulse is defined by three decision variables, a magnitude Δv_{LV} and two angles RLA and DLA that describe the right ascension and declination of the launch asymptote. Two additional decision variables, t_1 and η_1, encode the flight time for the first phase and the burn index, respectively. The burn index is a number in the range $[0.01, 0.99]$ that defines at what point along the spacecraft's arc the burn occurs. The spacecraft's initial state is defined as

$$\mathbf{r}_{s/c}\left(t_{launch}\right) = \mathbf{r}_{body}\left(t_{launch}\right) \tag{1}$$

$$\mathbf{v}_{s/c}\left(t_{launch}\right) = \mathbf{v}_{body}\left(t_{launch}\right) + \Delta v_{LV} \begin{bmatrix} \cos RLA \cos DLA \\ \sin RLA \cos DLA \\ \sin DLA \end{bmatrix} \tag{2}$$

The spacecraft's state vector is then propagated forward by $\eta_1 t_1$ days and then the deep space maneuver impulse is applied. The second half of the phase is modeled as a Lambert arc. The spacecraft must arrive at the next planet in the sequence at the end of that arc. The desired final position vector may be found by locating the planet at time $t = t_{launch} + t_1$. The flight time is simply $(1 - \eta_1)\, t_1$. Lambert's problem is solved to find the transfer arc, and the required deep space maneuver Δv_1 is just the magnitude of the vector difference between the spacecraft's velocity before and after entering the Lambert arc.

For every phase after the first, the process is very similar except that instead of starting with a propulsive maneuver, the remaining phases start with a flyby. The flyby is parameterized by two decision variables, the altitude ratio R_p and the b-plane insertion angle γ. The altitude ratio defines the periapse distance of the flyby r_p by

$$r_p = R_p r_{body} \tag{3}$$

where r_{body} is the radius of the planet. Then, knowing the incoming heliocentric velocity of the spacecraft, which is the same as its velocity at the end of the previous phase, and the mass of the planet, we can compute the velocity after the flyby. Once again we compute the incoming velocity of the spacecraft relative to the planet:

$$\mathbf{v}_{\infty/in} = \mathbf{v}_{sc/in} - \mathbf{v}_{body} \tag{4}$$

Because this flyby is unpowered, we assume that the spacecraft will follow a hyperbolic path about the planet and therefore the magnitudes of the incoming and outgoing velocity vectors relative to the planet are equal, *i.e.*,

$$v_{\infty/out} = v_{\infty/in} \tag{5}$$

The algorithm must then find the orientation of the outgoing velocity vector. First, the eccentricity of the hyperbola is found by

$$e = 1 + \frac{r_p \mathbf{v}_\infty^2}{G m_{body}} \tag{6}$$

and then the flyby transfer angle δ, shown in Figure 2, may be found by

$$\delta = 2 \sin^{-1}\left(1/e\right) \tag{7}$$

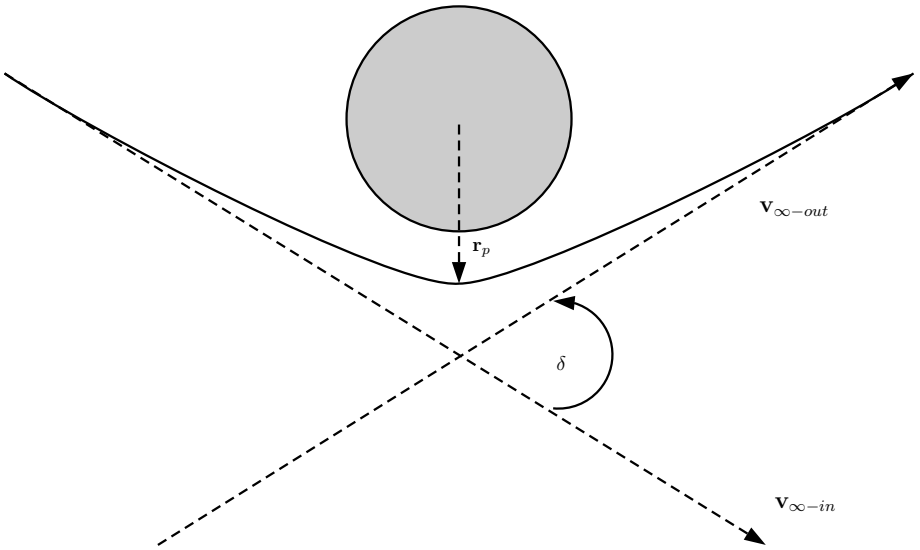

Figure 2: Definition of the flyby transfer angle δ

Finally, the incoming velocity vector must be rotated about the axis normal to the flyby hyperbola. The outgoing velocity vector is

$$\mathbf{v}_{\infty/out} = v_{\infty/in}\left(\cos\delta\hat{i} + \cos\gamma\sin\delta\hat{j} + \sin\gamma\sin\delta\hat{k}\right) \tag{8}$$

where $\hat{i}$, $\hat{j}$, $\hat{k}$ are the unit vectors defining the b-plane:

$$\hat{i} = \frac{\mathbf{v}_{\infty/in}}{v_{\infty/in}} \tag{9}$$

$$\hat{j} = \frac{\hat{i} \times \mathbf{v}_{pl}}{\left\|\hat{i} \times \mathbf{v}_{pl}\right\|} \tag{10}$$

$$\hat{k} = \hat{i} \times \hat{j} \tag{11}$$

The outgoing heliocentric velocity vector can then be found as

$$\mathbf{v}_{sc/out} = \mathbf{v}_{\infty/out} + \mathbf{v}_{body} \tag{12}$$

As in the first phase of the mission, the spacecraft motion is then propagated in time by $\eta_i t_i$, after which time Lambert's problem is solved again to find the arc and associated deep space maneuver necessary to bring the spacecraft to the next planet in the sequence. If this planet is the last in the sequence, an intercept (flyby), rendezvous, or orbit insertion may be performed depending on the mission requirements.

The MGADSM problem may then be summarized as

$$\begin{array}{c} \text{Minimize } f(\mathbf{x}) \\ \text{where :} \\ \mathbf{x} = \begin{array}{cccccccccc} [t_{launch} & \Delta v_{LV} & RLA & DLA & t_1 & \ldots & t_{n-1} & \eta_1 & \ldots & \eta_{n-1} \\ R_{p2} & \ldots & R_{p(n-1)} & \gamma_2 & \ldots & \gamma_{n-1}] & & & & \end{array} \end{array} \tag{13}$$

$f(\mathbf{x})$ can be any relevant fitness function. A simple two-phase MGADSM mission is shown in Figure 3.

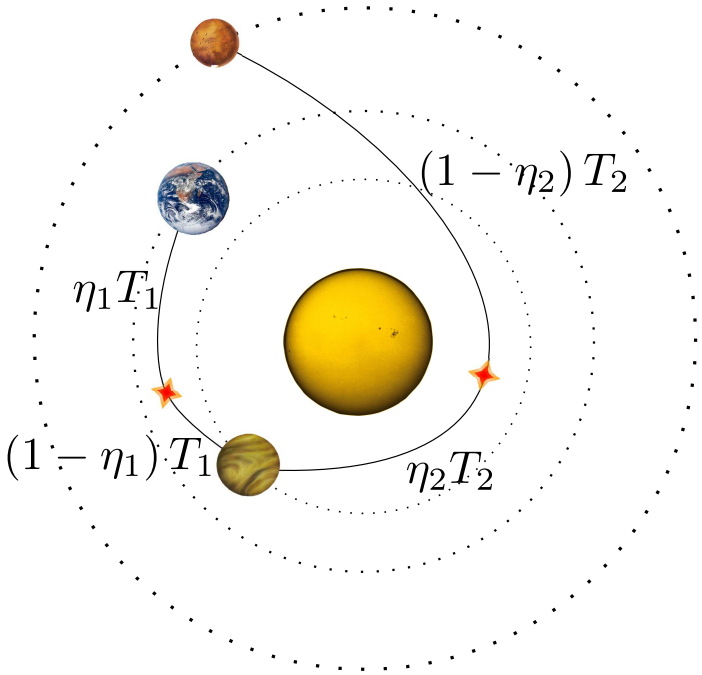

Figure 3: Diagram of a Two-Phase MGADSM Mission

Constraint Handling

A variety of constraints are considered in this work. There are two classes of constraints: constraints associated with feasibility of the trajectory model and constraints associated with the suitability of the trajectory for an actual mission.

The first feasibility constraint is on the energy of the spacecraft with respect to a flyby body at the moment of encounter, $C3_{flyby}$, where

$$C3_{flyby} = v_{\infty-in}^2 \tag{14}$$

For sufficiently small values of $C3_{flyby}$, Equation 6 yields an eccentricity very near zero even for an arbitrarily high periapse distance r_p. Equation 7 then yields an arbitrarily large, non-physical turn angle. One way to think of this conceptually is that for sufficiently small $C3_{flyby}$, the encounter orbit is nearly parabolic and the approximation of patching the heliocentric trajectory with a hyperbolic trajectory about the flyby body does not hold. It is possible to prevent this numerical singularity from affecting the trajectory design by imposing a nonlinear constraint on $C3_{flyby}$, *i.e.*,

$$C3_{flyby} \geq C3_{min} \tag{15}$$

A value of $C3_{min} = 0.1$ has been found empirically to work well.

The second model feasibility constraint deals with the well-known singularity in Lambert's problem for transfer angles of exactly 2π. This singularity, present in all solutions to Lambert's problem, leads to undefined, non-physical behavior at that precise transfer angle. While very few final trajectory designs will suffer from this problem, the optimizer needs to be able to "walk" through the entire problem space on the way to an answer. Therefore it is necessary that the optimizer have some knowledge of the fact that the transfer angle is approaching 2π so that it can avoid the singularity. In this work, this is done with a nonlinear constraint. Noting that the transfer angle $\theta_{Lambert}$ is given by,

$$\theta_{Lambert} = \arccos\left(\frac{\mathbf{r}_1 \cdot \mathbf{r}_2}{r_1 r_2}\right) \tag{16}$$

a transfer angle of 2π may be prevented by imposing a nonlinear constraint,

$$\frac{\mathbf{r}_1 \cdot \mathbf{r}_2}{r_1 r_2} \leq 1.0 \tag{17}$$

Constraints 15 and 17 ensure that the trajectory represented by the MGADSM model always reflects reality. The trajectory designer may wish to impose additional constraints that deal with the suitability of a trajectory solution for real-world use. Some of these constraints are straightforward, such as constraints on mission flight time, *i.e.*,

$$\sum_{i=1}^{n} t_i \leq t_{max} \tag{18}$$

or an upper bound on terminal velocity at intercept, *i.e.*,

$$v_{\infty - final} \leq v_{max} \tag{19}$$

However, other constraints are more complex. Different types of missions impose different operational constraints. For example, there may be a constraint that the spacecraft must approach a small body on the illuminated side, *i.e.* the angle between the $\mathbf{v}_\infty$ vector at arrival and the position vector of the body with respect the sun must be less than some threshold angle $\theta_{illumination}$, *i.e.*,

$$\arccos\left(\frac{\mathbf{v}_\infty \cdot \mathbf{r}_{body}}{v_\infty r_{body}}\right) \leq \theta_{illumination} \tag{20}$$

Such a constraint can enable science operations or possibly be translated into financial terms by allowing the spacecraft to fly with less capable sensors. This illumination constraint is just one of many possible operational constraints that could be imposed on a trajectory design problem. It is not sufficient to perform a global search on the unconstrained problem and then locally re-optimize on the constrained problem because the optimal solution to the constrained problem may not be in the neighborhood of the optimal solution to the unconstrained problem. Similarly, it is not efficient to solve many permutations of the unconstrained problem and then filter away solutions that do not satisfy the constraints because then it is too easy to filter away solutions that are almost feasible. Rather, it is better to include the operational constraints as part of the global search so that they can help shape the search process to be more efficient. This philosophy is followed in the second example presented in this work.

Objective Function, Launch Vehicle, and Ephemeris Modeling

Traditionally the objective function for a chemical mission is to minimize total Δv. This is because Δv can be added linearly, whereas Tsiolkovsky's rocket equation that governs spacecraft mass is exponential, *i.e.*,

$$m_f = m_0 e^{-\Delta v / I_{sp} g_0} \tag{21}$$

The linear quantity Δv is easier for a gradient-based optimizer to handle because its derivatives with respect to the decision variables are well behaved, whereas the derivatives of Equation 21 are not. However Equation 21 is not a completely accurate depiction of the cost of a mission because it does not take into account that the specific impulse (I_{sp}) of the spacecraft thrusters and of the launch vehicle are different, and therefore the same Δv performed by the launch vehicle affects the spacecraft differently from what would happen if that Δv were performed by the spacecraft itself.

Classically the different performance of the spacecraft and launch vehicle is handled by tracking two quantities, the Δv performed by the spacecraft and the characteristic energy, or $C3$, of the launch. $C3$ is defined as the square of the hyperbolic excess velocity of the spacecraft as it leaves the Earth. Many existing tools, such as STOUR [9], generate plots of $C3$ vs Δv. An analyst can then pick a point from the plot and compute the mass of the spacecraft as:

$$m_f = m_0 \left(C3\right) e^{-\Delta v / I_{sp} g_0} \tag{22}$$

where $m_0\,(C3)$ is the mass deliverable to a given $C3$ by the launch vehicle.

Plotting $C3$ vs Δv works reasonably well in a combinatorial exploration of the mission design space but does not work as well in a numerical optimization method such as the one presented in this work, because it is undesirable to have two different objective functions. One can use a multi-objective inner-loop solver to find the non-dominated front of $C3$ vs Δv, but there is a better way. The key is in finding a single metric that captures both $C3$ and Δv and has well-behaved derivatives. Optimizing on m_f directly accomplishes this, but as noted above the derivatives with respect to the problem decision variables are not well behaved; Equation 22 is essentially an exponential decay with an enormous decay constant.

Fortunately taking a logarithm of Equation 22 makes the derivatives much more stable. In this work, the objective function is:

$$J = -\log 10\,(m_f) = -log10\left(m_0\,(C3)\,e^{-\Delta v/I_{sp}g_0}\right) \tag{23}$$

This choice of objective function is inspired by the original formulation of Δv as a transformation of Equation 21 but is more appropriate to a mission in which maneuvering is accomplished by two different propulsion systems at different times as in Equation 22. The logarithm of 22 with respect to any base would probably work well, $\log 10$ is chosen for convenience and performs adequately.

Equation 23 requires a model of launch vehicle performance as a function of $C3$, which is provided as a 5^{th} degree polynomial:

$$m_{delivered} = (1-\sigma_{LV})\left(a_{LV}C_3^5 + b_{LV}C_3^4 + c_{LV}C_3^3 + d_{LV}C_3^2 + e_{LV}C3 + f_{LV}\right) \tag{24}$$

where σ_{LV} is the user-defined launch vehicle margin in $[0, 1]$ and the other coefficients are chosen by a curve fit to published launch vehicle performance data available at the Kennedy Space Center (KSC) expendable launch vehicle (ELV) performance website [28].

It is also necessary to provide accurate ephemeris modeling for all bodies used as destinations and/or flyby targets. Evolutionary Mission Trajectory Generator (EMTG) uses the SPICE toolkit [29] to provide this information when possible, and when SPICE kernels are not available it uses static orbit elements.

Lower and Upper Bounds

EMTG's stochastic optimizers require that the mission design problem be posed in a bounding box. If the bounds on the decision variables are too broad, the solvers will struggle to find a good solution. If the bounds are too negative than there is a risk of pruning away the optimal solution. Furthermore, because the trajectory design problem is being solved as the inner-loop of a HOCP, there is no opportunity for a human analyst to step in and set appropriate bounds for every possible problem. Therefore a set of simple rules are used to determine the bounds as shown in Table 1.

Table 1: Automated Choosing of Inner-Loop Bounds for MGADSM Problems

Parameter	Lower Bound	Upper Bound
Launch date	user-defined	user-defined
Stay time between journeys	user-defined	user-defined
RLA	0.0	2π
DLA	user-defined	user-defined
$v_{\infty-launch}$	0.0	user-defined
For each phase:		
Flight time:		
(repeated flyby of same planet)	$T/2$ (repeated flyby of same planet)	$20T$
(outermost body has $a < 2LU$)	$0.1min\left(T_1, T_2\right)$	$2.0max\left(T_1, T_2\right)$
(outermost body has $a \geq 2LU$)		$max\left(T_1, T_2\right)$
Burn index η	0.01	0.99
B-plane insertion angle γ	$-\pi$	π
Flyby periapse distance ratio R_p	$1.0 + h_{max}/R_{body}$	10 (rocky bodies) 300 (gas giants)

OUTER-LOOP OPTIMIZATION OF THE MISSION SEQUENCE

Outer-Loop Transcription

The mission design problem in this work is posed as two nested optimization problems, an "outer-loop" discrete optimization problem and an "inner-loop" real-valued optimization problem. The outer-loop solves a multi-objective integer programming problem whose candidate solutions are themselves instances of the inner-loop trajectory optimization problem. The outer-loop works via a "cap and optimize" process by which it chooses design variables such as destinations, flybys, and bounds on the launch date and flight time that define a tractable inner-loop subproblem.

The user specifies *a priori* a list of outer-loop design variables and a "menu" of choices with corresponding integer codes for each. In this work the design variables are launch epoch, time of flight, destinations, and flybys. The outer-loop algorithm makes one choice from each menu.

Launch epoch is transcribed as a menu of candidate launch dates plus a launch window size. For example, the user might specify launches in 2020, 2021, or 2022 with a 365 day launch window. The outer-loop chooses one of the available launch years and constructs an inner-loop problem where the spacecraft can depart Earth at any time during that year. The method for time of flight is similar - the user specifies a list of flight times and the optimizer chooses one and sets it as the upper-bound for the inner-loop problem. No lower-bound is enforced - this seems to yield a more tractable inner-loop problem.

The user may also specify a menu of candidate destinations for each journey. For example, one might wish to design a mission to two asteroids but have a long list of scientifically interesting options. The HOCP automaton can choose the most accessible asteroids. The outer-loop may be instructed to discard candidate solutions that visit the same destination body more than once.

Flyby sequence selection is similar to journey destination selection except that one does not always know how many flybys are to be performed. A "null-gene" technique is used to choose the number and identity of flyby bodies [17]. The analyst provides a list of acceptable flyby bodies and a maximum number of flybys for each journey. Then, for each potential flyby, the outer-loop may select from a list containing the specified acceptable bodies and also a number of "null" options equal to the number of acceptable bodies. The outer-loop therefore has an equal probability of selecting "no flyby" for each opportunity as it does to select a flyby. This technique has been shown to be very effective for designing multi-flyby interplanetary missions and has been used to reproduce the Cassini [17] trajectory and design an efficient variant of the BepiColombo trajectory [30].

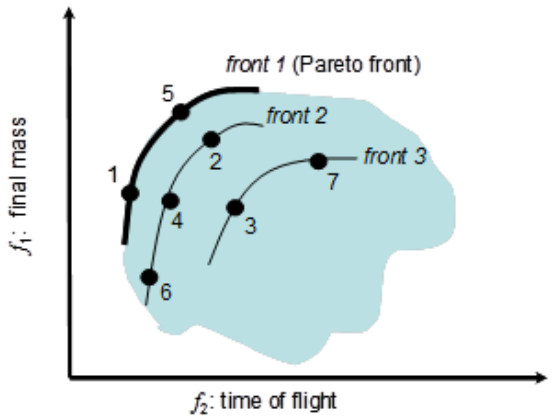

Figure 4: Two-Dimensional, Non-Dominated Fronts of a Multi-Objective Trajectory Optimization Example

The user may then select any number of outer-loop objective functions for optimization. Some of these, such as flight time and launch year, may be directly related to decision variables. Others, such as final mass, may be the product of an the inner-loop optimization process. The inner-loop subproblem is optimized over only one objective function but because the "cap and optimize" outer-loop constrains the inner-loop, each sub-problem solution is a candidate solution to the multi-objective outer-loop problem.

Outer-Loop Multi-Objective Optimization via NSGA-II

The goal of multi-objective optimization is to generate the Pareto front of solutions [31]. The Pareto front represents the set trade-off solutions in which no improvement can be achieved in one objective without degrading at least one other objective. That is, all designs that compose the Pareto front are equally optimal. The Pareto front can be discontinuous and either concave or convex. Thus, the aim of multi-objective optimization is to generate numerous Pareto-optimal solutions such that a representation the Pareto front is created to enable a tradeoff decision. The Pareto front for a notional low-thrust trajectory optimization problem with the objectives to maximize final spacecraft mass and minimize time of flight is illustrated in Figure 4. The multi-objective optimization problem can be stated as:

$$\begin{aligned} &\text{minimize } \mathbf{f}(\mathbf{x}) \\ &\text{subject to } \mathbf{c}(\mathbf{x}) \leq \mathbf{0} \\ &\qquad \mathbf{x}_{LB} \leq \mathbf{x} \leq \mathbf{x}_{UB} \end{aligned} \tag{25}$$

where $\mathbf{f}(\mathbf{x})$ is a vector of objective functions, $\mathbf{x}$ is a vector of design variables, $\mathbf{c}(\mathbf{x})$ is a vector of constraint functions, and $\mathbf{x}_{LB}$ and $\mathbf{x}_{UB}$ are vectors of upper and lower bounds for $\mathbf{x}$, respectively. The objective functions are often coupled, *i.e.* contain the same design variables, and also competing, *i.e.* the optimal solution with respect to one objective is not also the optimal solution with respect to the other objectives. Competition between objectives creates the need to find multiple solutions, making multi-objective optimization more complex than single-objective optimization. The outer-loop of this work uses bounded but unconstrained multi-objective optimization, with the constraints $\mathbf{c}$ handled by the single-objective inner-loop.

The multi-objective optimization concept of domination allows for the comparison of a set of designs with multiple objectives, providing a measure of the relative quality of the design. When comparing two multi-objective designs, the design $\mathbf{x}_1$ dominates design $\mathbf{x}_2$ if:

$$\begin{aligned} &\forall p : f_p(\mathbf{x}_1) \leq f_p(\mathbf{x}_2) \quad \text{where} \quad p = 1, 2, ...n_{objectives} \\ &\exists p : f_p(\mathbf{x}_1) < f_p(\mathbf{x}_2) \end{aligned} \tag{26}$$

That is, $\mathbf{x}_1$ dominates design $\mathbf{x}_2$ if, for all objectives p, $\mathbf{x}_1$ is better than or equal to $\mathbf{x}_2$, and $\mathbf{x}_1$ outperforms $\mathbf{x}_2$ for at least one objective. In a direct comparison of two designs, if one design dominates another, that

design is closer in proximity to the Pareto front. If neither design dominates the other, the designs are non-dominant to each other. Therefore, in a set of designs, the superior designs are those that are not dominated by any other design in the set, and are termed the non-dominated subset. It follows that any Pareto-optimal design is a member of the non-dominated subset associated with the entire feasible objective space and is located along the Pareto front. A solution space with several Pareto fronts is shown in Figure 4.

A multi-objective genetic algorithm (MOGA) is an appropriate solution method for the outer-loop problem. A GA is a stochastic search and optimization technique that simulates natural selection and reproduction with the goal of identifying globally-optimal designs. A GA first generates a random population of designs and then iteratively executes three genetic operators: selection, crossover, and mutation. The operators are applied to a parent population to produce a new offspring generation that is better adapted to fitness landscape defined by the objective functions. A GA does not require an initial guess or gradient information, making it ideal for exploring discrete, multi-modal, and expansive design spaces. A MOGA is a modified version of the standard GA that can solve multi-objective problems.

A MOGA is capable of finding the Pareto front for a multi-objective problem in a single optimization run. This is more efficient, in terms of computer time required, than performing many repetitions of a single-objective optimization routine. One effective MOGA is the Non-Dominated Sorting Genetic Algorithm (NSGA) developed by Deb [32], in which the fitness of an individual in the population is based on its relative proximity to the population's non-dominated front. The genetic operators of the NSGA evolve the population toward the globally-optimal Pareto front in the same way that the population of a single-objective GA evolves toward the globally optimal solution.

A second generation non-dominated sorting genetic algorithm, the NSGA-II, improves upon the original NSGA [25]. The NSGA-II incorporates mechanisms that ensure that the elite individuals, *i.e.* the best individuals in the population, are retained as the population evolves. Additionally, the NSGA-II employs strategies that aim to produce a uniform representation of designs along the Pareto front. Domination is used to categorize each design into non-dominated fronts. The solutions composing the best non-dominated front are given a rank of one, and each subsequent front is given an incrementally higher rank according to their relative distance to the Pareto front. The fast non-dominated sorting algorithm by Deb is outlined in Algorithm 1, where m and n are individual solutions, S_m is the set of solutions that dominate m, c_m is the number of solutions that dominate m, F_i are sets that contain the non-dominated fronts, Q is a temporary set, and n_{rank} is rank of solution n.

The NSGA-II preserves diversity by preferring the solution that is in a less dense region of the objective function space when comparing two solutions of the same rank. A crowding distance is assigned to each individual based on the perimeter of the hyper-rectangle formed with the two adjacent designs in objective space for each of each objective. The HOCP automaton described in this work employes a modified version of Deb's [25] crowding distance assignment to accommodate instances in which there are more than two objectives and there are multiple solutions belonging to the same non-dominated front with the same minimum objective function value. Whenever there are multiple solutions that take the minimum or maximum value for a given objective function coinciding in the same non-dominated front, the solutions with the lowest objective function value for the other objectives are given a large crowding distance. The remaining solutions in the boundary group are assigned a crowding-distance based on a single adjacent solution for each objective. This approach ensures that solutions with a minimum objective function value will not be discarded if the entire population composes a single non-dominated front. The modified crowding distance assignment operator is described in Algorithm 2, where I is the set of solutions to be sorted and the operator $sort\,(I, p)$ refers to sorting a list I in ascending order by objective p. L is the set of solutions for a given objective p for which p is at a minimum and H is the set of solutions for which p is at a maximum, at the current generation.

After ranking the population using the non-dominated sort and crowding distance algorithms, NSGA-II applies genetic operators to the parent population to create an offspring population of the same size N. The parent and offspring populations are then combined into a single population of size $2N$. This combined population is then sorted and ranked according to non-domination. The next generation's parent population is created by taking each non-dominated front from the combined population, in rank order, until the new

Algorithm 1 Fast non-dominated sort [25]

```
for each individual m in population P do
    S_m = ∅
    c_m = 0
    for each individual n in population P do
        if m dominates n then
            S_m = S_m ⋃ {n}
        else if n dominates m then
            c_m = c_m + 1
        end if
    end for
    if c_m = 0 then
        m_rank = 1
        F_1 = F_1 ⋃ {m}
    end if
end for
i = 1
while F_i ≠ ∅ do
    Q = ∅
    for each individual m in front F_i do
        for each individual n in S_m do
            c_m = c_m − 1
            if c_m = 0 then
                n_rank = i + 1
                Q = Q ⋃ {n}
            end if
        end for
    end for
    i = i + 1
    F_i = Q
end while
```

parent population is filled. In this way the preservation of elite individuals is guaranteed and diversity in objective space is promoted. The process is repeated for a set number of generations or length of time.

The NSGA-II is well-suited for the multi-objective trajectory optimization problem: it is capable of generating the Pareto front to illustrate the trade-offs in the mission objectives of interest, can globally search the design, and is automated without requiring an initial guess.

Parallel Outer-Loop Optimization

The evaluation of the objective functions for a candidate solution is very expensive - it requires solving the entire inner-loop trajectory optimization problem and can take at best several seconds, in most cases many minutes, and in some cases hours. Fortunately each inner-loop subproblem is independent of the others so it is natural to evaluate them in parallel. The pool of *N* inner-loop subproblems to be evaluated is distributed over *P* processor cores. If *N* exceeds *P*, the subproblems are agglomerated into *P* task pools with one assigned to each processor. The run-time is further decreased by saving each candidate solution to the outer-loop problem so that none must be evaluated more than once. Therefore the number of inner-loop instances to be run for each outer-loop generation tends to decrease and the algorithm speeds up with each generation of NSGA-II.

There are two parallel processing paradigms: shared memory multiprocessing and distributed memory multicomputing. Shared memory multiprocessing, also known as threading, is easier to implement but is not appropriate for this work because it requires all processes to be "thread-safe," *i.e.* do not interfere with

Algorithm 2 Modified Crowding-Distance Assignment

for each objective p **do**
  $I_p = sort\left(I, p\right)$
  $L = \emptyset$
  $H = \emptyset$
  for i in I_p **do**
    if $p = 0$ **then**
      $I_p\left[i\right]_{distance} = 0$
    end if
    if $f_p\left(I_p\left[i\right]\right) = f_p^{min}$ **then**
      $A \bigcup B$
      $L = L \bigcup \{I_p\left[i\right]\}$
    else if $I_p\left[i\right]_{objective-value} = f_p^{max}$ **then**
      $H = \bigcup H, \{I_p\left[i\right]\}$
    else
      $I_p\left[i\right]_{distance} = I_p\left[i\right]_{distance} + \left(f_p\left(I_p\left[i+1\right]\right) - f_p\left(I_p\left[i-1\right]\right)\right) / \left(f_p^{max} - f_p^{min}\right)$
    end if
  end for
  for each objective q except p **do**
    $L_q = sort\left(L, q\right)$
    $L_q\left[0\right]_{distance} = \infty$
    $H_q = sort\left(L, q\right)$
    $H_q\left[0\right]_{distance} = \infty$
  end for
end for

each other even while operating in the same memory space. However the SPICE ephemeris reader used in this work is not thread-safe and therefore the entire algorithm cannot be used with shared memory multiprocessing. Instead the algorithm described in this work is implemented using the distributed memory multicomputing library message passing interface [33] in which each processor runs an independent process in distinct memory spaces.

INNER-LOOP TRAJECTORY OPTIMIZATION

Stochastic Global Search via Monotonic Basin Hopping and SNOPT

Because the solutions to the outer-loop problem require solutions to the inner-loop trajectory optimization subproblem, the performance of the HOCP automaton is only as good as the performance of the inner-loop solver. A solver is required that can solve large, multi-modal problems with many nonlinear constraints. Because the inner-loop problem is generated in real time by the outer-loop, the inner-loop solver cannot require any human intervention and therefore cannot require an initial guess - a natural application for a heuristic stochastic search. The HOCP automaton described in this work uses monotonic basin hopping (MBH) [26, 34, 27, 7]. MBH, described in Algorithm 3, is a hybrid of a stochastic search step with an nonlinear programming (NLP) solver. The stochastic search step efficiently explores the space and the NLP step enforces the constraints and exploits local basins. The NLP step makes MBH particularly adept at handling challenging constraints such as the illumination angle constraint in Equation 20. The NLP step in this work is performed using Sparse Nonlinear Optimizer (SNOPT) [35].

The MBH+NLP optimization algorithm in EMTG is efficient and does not require an initial guess. MBH is most useful when one does not have much *a priori* information about the solution as is *always* the case when solving an inner-loop trajectory optimization problem inside a hybrid optimal control (HOC) mission design problem.

Algorithm 3 Monotonic Basin Hopping (MBH)

generate random point $\mathbf{x}$
run NLP solver to find point $\mathbf{x}^*$ using initial guess $\mathbf{x}$
$\mathbf{x}_{current} = \mathbf{x}^*$
if $\mathbf{x}^*$ is a feasible point **then**
  save $\mathbf{x}^*$ to archive
end if
while not hit stop criterion **do**
  generate $\mathbf{x}'$ by randomly perturbing $\mathbf{x}_{current}$
  for each time of flight variable t_i in $\mathbf{x}'$ **do**
    if $rand\,(0,1) < \rho_{time-hop}$ **then**
      shift t_i forward or backward one synodic period
    end if
  end for
  run NLP solver to find point $\mathbf{x}^*$ from $\mathbf{x}'$
  if $\mathbf{x}^*$ is feasible **and** $f\,(\mathbf{x}^*) < f\,(\mathbf{x}_{current})$ **then**
    $\mathbf{x}_{current} = \mathbf{x}^*$
    save $\mathbf{x}^*$ to archive
  else if $\mathbf{x}^*$ is infeasible **and** $\|c\,(\mathbf{x}^*)\| < \|c\,(\mathbf{x}_{current})\|$)
    $\mathbf{x}_{current} = \mathbf{x}^*$
  end if
end while
return best $\mathbf{x}^*$ in archive

EXAMPLES

Jupiter Probe

In the first example, EMTG is used to design a notional mission to Jupiter in the 2020s. The spacecraft is to arrive at Jupiter and insert into an elliptical orbit with a semi-major axis of 140 R_J and an eccentricity of 0.91. Some sequence of tour of Jupiter's moons would then be conducted but is out of scope of this work, which focuses only on the interplanetary trajectory. The problem assumptions and solver settings for the Jupiter example are shown in Table 2.

The outer-loop was run for 500 generations on a 64-core AMD Opteron running at 2.6 GHz, which took two days and required no human interaction other than a few minutes to set up the initial problem. EMTG considered 8893 candidate outer-loop solutions, a non-dominated set of which are shown in Figure 5. Each point in Figure 5 represents a completely different mission, including launch date, flight time, propulsive maneuvers, and flybys. Two representative missions are shown in Figure 6. Figure **??**(a) represents a mission which launches in 2021 but takes 8 years to deliver 2932 kg to Jupiter, while the mission in Figure **??***(*b) launches in 2026 and because of more favorable geometry delivers 3180 kg in only 5 years.

Whack-a-Rock

The second example presented here is a complex mission to deliver a high-velocity penetrator probe to a C-type near-Earth object (NEO) and then circle back around, rendezvous with the NEO, and inspect the impact site in detail. This example is inspired by NASA's Deep Impact mission, which delivered a penetrator probe to comet Tempel 1 in 2005 [36]. One objective was to image the impact site but unfortunately so much dust was thrown up that it could not be resolved. Unfortunately it was not possible to send Deep Impact back to Tempel 1 for a second look, so a second spacecraft, the re-purposed Stardust spacecraft was later sent to perform the observations [37]. In this example, hybrid optimal control is used to choose a target specifically for "re-accessibility."

The set of allowable targets for the "Whack-a-Rock" mission is all NEOs of spectral type C and at least 500

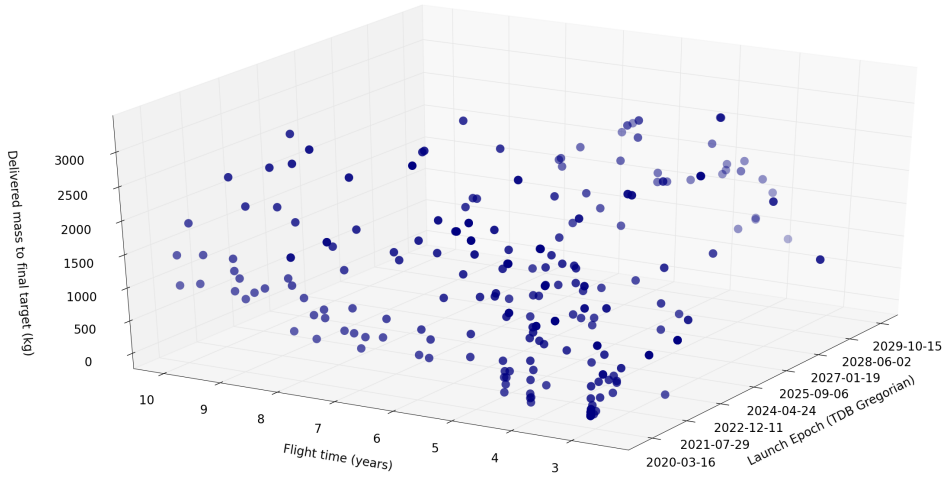

Figure 5: Final generation of NSGA-II for the Jupiter Probe example

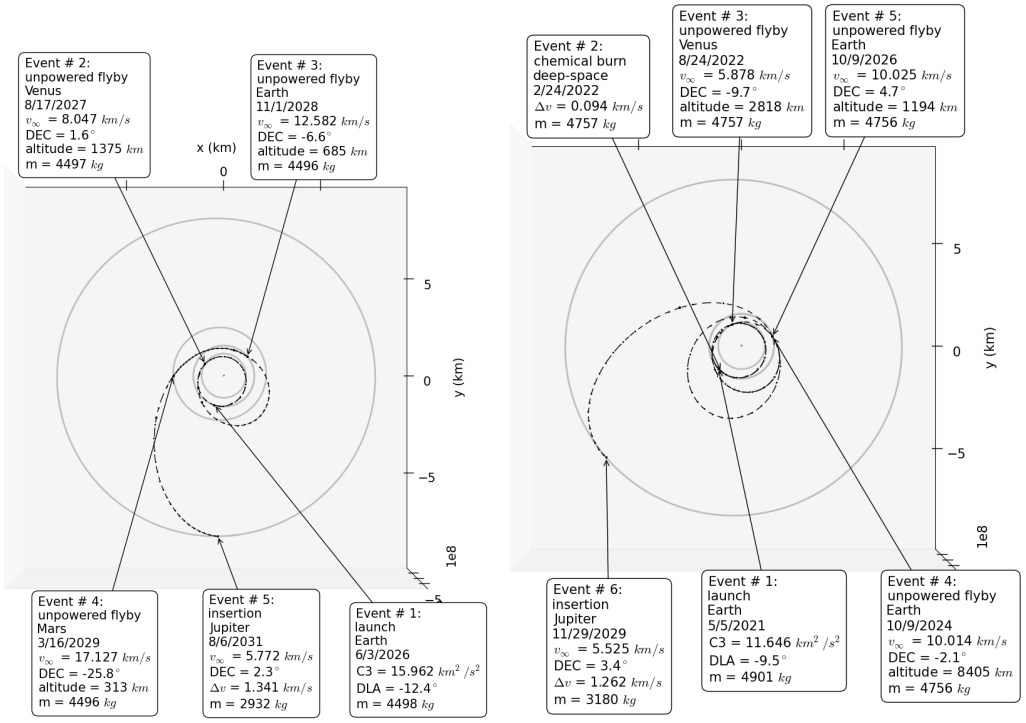

(a) 8-year mission launching in 2021

(b) 5-year mission launching in 2026

Figure 6: Example Jupiter missions

Table 2: Assumptions and Settings for the Jupiter Probe Example

Description	Value
Launch year	outer-loop chooses $\in [2020, 2029]$
Flight time	outer-loop chooses $\in [3, 10]$ years
Launch vehicle	Atlas V 551
Spacecraft I_{sp}	320 s
Arrival condition	insert into orbit at Jupiter
	$a = 140R_J$
	$e = 0.91$
Number of flybys allowed	5
Flyby targets considered	Venus, Earth, Mars
Outer-loop objective functions	launch year
	flight time
	delivered mass
Outer-loop population size	256
Outer-loop mutation rate	0.3
Inner-loop MBH run-time	10 minutes
Inner-loop MBH Pareto α	1.3

meters in diameter, as defined by the JPL small bodies database [38]. There are 25 targets in this list, as shown in Table 3. Whack-a-Rock is modeled in EMTG as a mission with two journeys, the first being from the Earth to the target and the second being to return to and rendezvous with the target. Up to two flybys of Venus, Earth, and/or Mars are allowed in each journey. The first journey ends in an intercept, *i.e.* a match of position but not velocity, with two constraints imposed. The first constraint is that the velocity magnitude at impact be between 5 and 10 km/s. If the penetrator is too slow, it will not make an adequate crater. If it is too fast, its sampling instruments will not work. The second constraint is that the angle between the probe's terminal velocity and the target's position with respect to the sun must be less than 70° as described in Equation 20. This ensures that the target is sufficiently illuminated for the penetrator's terminal guidance system to work. Both of these constraints are incorporated into the inner-loop problem. The full set of problem assumptions is shown in Table 4.

Once again EMTG was run for 350 generations on a 64-core AMD Opteron running at 2.6 GHz, with a total run time of about 3.8 days. EMTG evaluated 25141 candidate solutions, a non-dominated front of which are shown in Figure 7. Each point in Figure 7 represents a different combination of target, flybys, launch vehicle, launch year, and flight time. The choice of launch vehicle is shown on the color axis, with redder being a larger launch vehicle.

Two of the many possible missions are shown in Figure 8. Both missions meet the Whack-a-Rock mission objectives by delivering a probe with the required impact velocity and illumination angle and both deliver more than 2500 kg to rendezvous. However the two examples represent very different approaches to the problem. One accomplishes the mission in a short time using the Atlas V 551 launch vehicle, and the other accepts a much longer flight time in exchange for the less expensive Atlas V 421. Depending on the needs of the customer, *i.e.* whether the cost of a larger launch vehicle is greater than or less than the cost of additional flight time or alternatively depending on which candidate NEO is most scientifically attractive, any mission in Figure 7 could be chosen for detailed analysis and eventually flight.

CONCLUSION

Summary

In this work we show that the impulsive-thrust interplanetary mission design problem may be posed as a multi-objective HOCP and efficiently explored via the powerful combination of a multi-objective discrete

Table 3: Allowable targets for the "Whack-a-Rock" mission

Name	a (AU)	e	$i\,(^\circ)$	$\Omega\,(^\circ)$	$\omega\,(^\circ)$
2100 Ra-Shalom	0.83	0.44	15.76	170.84	356.04
3671 Dionysus	2.20	0.54	13.55	82.16	204.20
3691 Bede	1.77	0.28	20.36	348.77	234.88
14402 1991DB	1.72	0.40	11.42	158.26	51.32
15817 Lucianotesi	1.32	0.12	13.87	162.52	94.30
16064 Davidharvey	2.85	0.59	4.54	335.61	104.84
65706 1992NA	2.40	0.56	9.71	349.38	8.10
85774 1998UT18	1.40	0.33	13.59	64.71	50.01
136793 1997AQ18	1.15	0.47	17.38	296.30	36.98
141079 2001XS30	1.16	0.83	28.53	251.47	0.87
152563 1992BF	0.91	0.27	7.27	315.57	336.30
152679 1998KU2	2.25	0.55	4.93	205.79	120.28
162173 1999JU3	1.19	0.19	5.88	251.61	211.43
162567 2000RW37	1.25	0.25	13.75	333.34	133.26
175706 1996FG3	1.05	0.35	1.99	299.73	23.99
308635 2005YU55	1.16	0.43	0.34	35.89	273.63
322775 2001HA8	2.39	0.53	11.48	95.89	202.37
370061 2000YO29	1.81	0.69	54.60	262.66	309.32
413123 2001XS1	2.67	0.56	10.93	266.97	164.88
1997 AC11	0.91	0.37	31.64	116.94	141.62
1998 HT31	2.52	0.69	6.80	213.91	80.42
1999 VN6	1.73	0.37	19.48	58.10	43.56
2000 WL10	3.14	0.72	10.24	252.16	115.12
2001 SJ262	2.94	0.58	10.80	210.44	164.93
2002 DH2	2.05	0.54	20.94	345.56	231.79

Table 4: Assumptions and Settings for the Whack-a-Rock Example

Description	Value
Launch year	outer-loop chooses $\in [2020, 2029]$
Flight time	outer-loop chooses $\in [3, 12]$ years
Launch vehicle	outer-loop chooses Atlas V 401, 411, 421, 431, 541, or 551
Spacecraft I_{sp}	320 s
Penetrator mass	20 kg
Arrival conditions	
(first Journey)	intercept with $v_\infty \in [5.0, 10.0]\,km/s$, $\theta_{illumination} \leq 70^\circ$
(second Journey)	rendezvous
Number of flybys allowed	2 in each Journey
Flyby targets considered	Venus, Earth, Mars
Outer-loop objective functions	launch year
	flight time
	delivered mass
	launch vehicle choice
Outer-loop population size	256
Outer-loop mutation rate	0.3
Inner-loop MBH run-time	10 minutes
Inner-loop MBH Pareto α	1.3

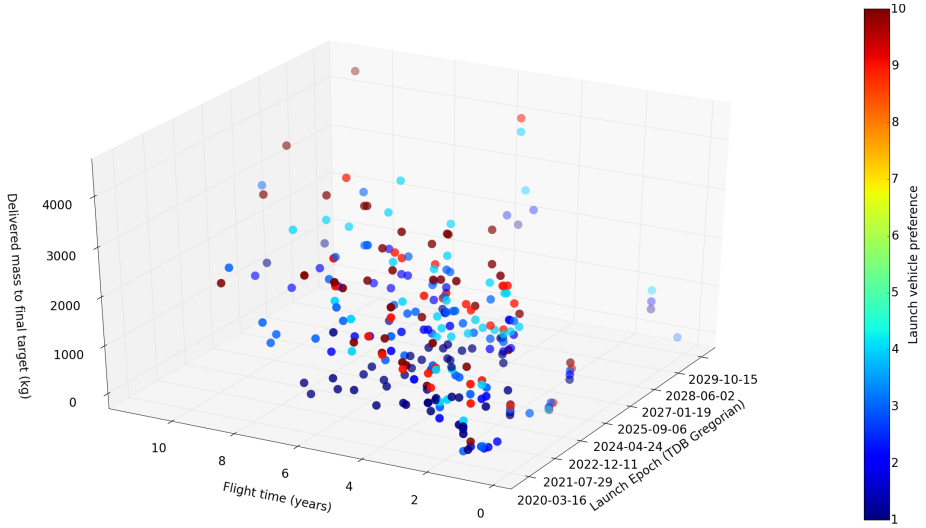

Figure 7: Final generation of NSGA-II for the Whack-a-Rock example

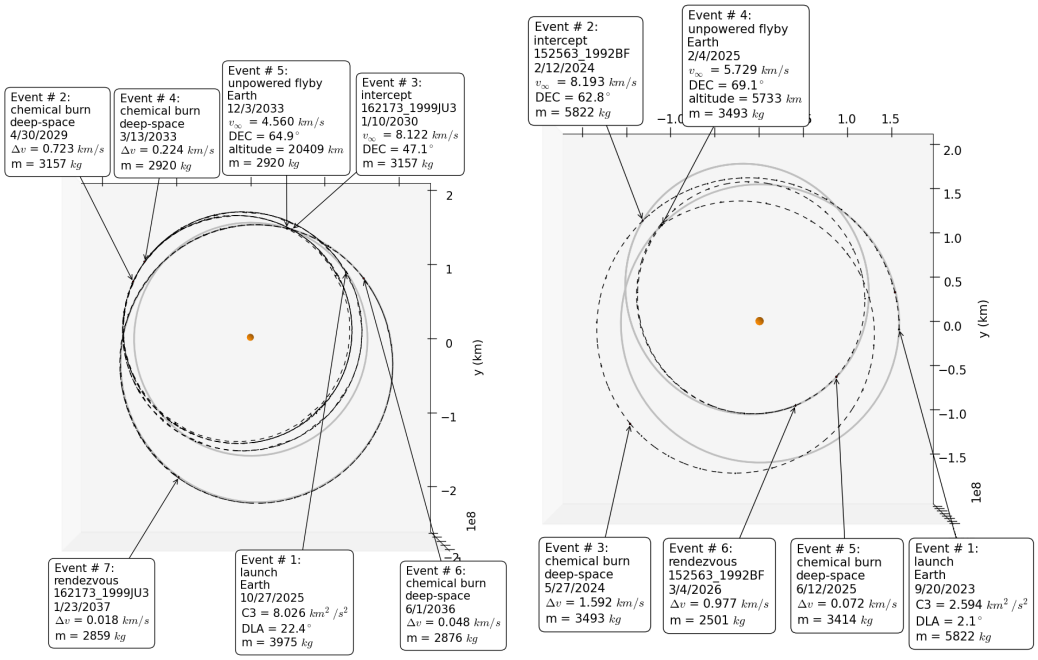

(a) 2501 kg delivered to 1999 JU3 on Atlas V 421 in 11.25 years

(b) 2859 kg delivered to 1992 BF on Atlas V 551 in 2.45 years

Figure 8: Example Whack-a-Rock missions

NSGA-II outer-loop with a MBH+NLP inner-loop. The trade space for a given mission and spacecraft design may be characterized even when there is only enough time to evaluate a fraction of the full combinatorial design problem. The HOCP automaton presented here is shown very effective in exploring the design spaces for a notional Jupiter probe and a very complex mission to impact and then revisit an NEO. Furthermore the HOCP automaton is found to handle complex operational constraints such as the target illumination constraint.

The algorithm described here is in use at NASA Goddard Space Flight Center and offers three compelling advantages. First, multiple mission cases may now be studied simultaneously, limited only by available computing power. Second, mission design engineers can now spend more time with the customer and with spacecraft hardware engineers so that they can fully understand the scientific and engineering context of their work and deliver better value to the customer. Third, good mission ideas are much less likely to be rejected due to lack of time to work on mission design, and bad ideas are much more likely to be rejected before they consume too many resources because the full space of "what if" options may be explored autonomously before a large team of specialists is brought to bear.

The algorithms described in this work are available as part of the open-source EMTG project [39]. The authors encourage the reader to examine and use them and welcome opportunities for collaboration with researchers from all backgrounds.

ACKNOWLEDGMENTS

The authors would like to acknowledge Donald Ellison and Professor Bruce Conway at the University of Illinois for their ongoing contributions to the algorithms behind EMTG and hybrid optimal control in general. The authors would also especially like to thank David Hinckley of the University of Vermont for discovering the need for a nonlinear constraint on Lambert transfer angle.. This research was funded by the NASA Goddard independent research and development program.

REFERENCES

[1] J. Prussing and B. Conway, *Orbital Mechanics*. Oxford University Press, New York, 1993.

[2] M. Vasile and P. De Pascale, "Preliminary Design of Multiple Gravity-Assist Trajectories," *Journal of Spacecraft and Rockets*, Vol. 43, No. 4, 2006, pp. 794–805.

[3] A. D. Olds, C. A. Kluever, and M. L. Cupples, "Interplanetary mission design using differential evolution," *Journal of Spacecraft and Rockets*, Vol. 44, No. 5, 2007, pp. 1060–1070.

[4] T. Vinkó and D. Izzo, "Global Optimisation Heuristics and Test Problems for Preliminary Spacecraft Trajectory Design," Tech. Rep. GOHTPPSTD, European Space Agency, the Advanced Concepts Team, 2008.

[5] M. Schlueter, J. Rckmann, and M. Gerdts, "Non-linear mixed-integer-based Optimisation Technique for Space Applications," Poster for ESA NPI Day, 2010.

[6] M. Vasile, E. Minisci, and M. Locatelli, "Analysis of some global optimization algorithms for space trajectory design," *Journal of Spacecraft and Rockets*, Vol. 47, No. 2, 2010, pp. 334–344.

[7] J. A. Englander and A. C. Englander, "Tuning Monotonic Basin Hopping: Improving the Efficiency of Stochastic Search as Applied to Low-Thrust Trajectory Optimization," *24th International Symposium on Space Flight Dynamics, Laurel, MD*, May 2014.

[8] B. Barbee, P. Abell, D. Adamo, C. Alberding, D. Mazanek, L. Johnson, D. Yeomans, C. P. W., A. Chamberlin, and V. Friedensen, "The Near-Earth Object Human Space Flight Accessible Targets Study: An Ongoing Effort to Identify Near-Earth Asteroid Destinations for Human Explorers," *2013 IAA Planetary Defense Conference*, April 2013.

[9] J. Longuski and S. Williams, "Automated design of gravity-assist trajectories to Mars and the outer planets," *Celestial Mechanics and Dynamical Astronomy*, Vol. 52, No. 3, 1991, pp. 207–220.

[10] J. Downing, "Pyxis Tool," Tech. Rep. NASA/TM-2006-214139, Flight Dynamics Branch (FDAB), NASA Goddard Space Flight Center, August 2006.

[11] A. Gad and O. Abdelkhalik, "Hidden Genes Genetic Algorithm for Multi-Gravity-Assist Trajectories Optimization," *Journal of Spacecraft and Rockets*, Vol. 48, July-August 2011, pp. 629–641.

[12] O. Abdelkhalik and A. Gad, "Dynamic-Size Multi-Population Genetic Optimization for Multi-Gravity-Assist Trajectories," *Journal of Guidance, Control, and Dynamics*, Vol. 35, March-April 2012, p. 520529.

[13] M. Vasile and S. Campagnola, "Design of low-thrust multi-gravity assist trajectories to Europa," *Journal of the British Interplanetary Society*, Vol. 62, No. 1, 2009, pp. 15–31.

[14] M. Buss, M. Glocker, M. Hardt, O. v. Stryk, R. Bulirsch, and G. Schmidt, "Nonlinear Hybrid Dynamical Systems: Modeling, Optimal Control, and Applications," *Lecture Notes in Control and Information Sciences*, Vol. 279, 2002, pp. 311–335.

[15] I. M. Ross and C. D'Souza, "Hybrid Optimal Control Framework for Mission Planning," *Journal of Guidance, Control, and Dynamics*, Vol. 28, July-August 2005, pp. 686–697.

[16] B. Conway, C. Chilan, and B. Wall, "Evolutionary principles applied to mission planning problems," *Celestial Mechanics and Dynamical Astronomy*, Vol. 97, No. 2, 2007, pp. 73 – 86.

[17] J. Englander, B. Conway, and T. Williams, "Automated Mission Planning via Evolutionary Algorithms," *Journal of Guidance, Control, and Dynamics*, Vol. 35, No. 6, 2012, pp. 1878–1887.

[18] J. A. Englander, *Automated Trajectory Planning for Multiple-Flyby Interplanetary Missions*. PhD thesis, University of Illinois at Urbana-Champaign, April 2013.

[19] V. Coverstone-Carroll, J. Hartmann, and W. Mason, "Optimal multi-objective low-thrust spacecraft trajectories," *Computer Methods in Applied Mechanics and Engineering*, Vol. 186, No. 24, 2000, pp. 387 – 402.

[20] M. Vavrina and K. Howell, "Multiobjective Optimization of Low-Thrust Trajectories Using a Genetic Algorithm Hybrid," *AAS/AIAA Space Flight Mechanics Meeting*, February 2009. AAS 09-141.

[21] M. Vasile and F. Zuiani, "MACS: A hybrid multiobjective optimization algorithm applied to space trajectory optimization, Journal of Aerospace Engineering," *Proceedings of the Institution of Mechanical Engineers Part G*, Vol. 225, 2011, pp. 1211–1227.

[22] D. Izzo, D. Hennes, and A. Riccardi, "Constraint Handling and Multi-Objective Methods for the Evolution of Interplanetary Trajectories," *AIAA Journal of Guidance, Control, and Dynamics*, Vol. 4, 2014, pp. 792–799.

[23] J. Englander, M. Vavrina, and A. Ghosh, "Multi-Objective Hybrid Optimal Control for Multiple-Flyby Low-Thrust Mission Design," *AAS/AIAA Space Flight Mechanics Meeting*, January 2015.

[24] M. Vavrina, J. Englander, and A. Ghosh, "Coupled Low-Thrust Trajectory and Systems Optimization Via Multi-objective Hybrid Optimal Control," *AAS/AIAA Space Flight Mechanics Meeting*, January 2015. AAS 15-397.

[25] K. Deb, S. Agrawal, A. Pratap, , and T. Meyarivan, "A fast and elitist multi-objective genetic algorithm: NSGA-II," *IEEE Transactions on Evolutionary Computation*, Vol. 6, April 2002, pp. 182–197.

[26] R. Leary, "Global optimization on funneling landscapes," *Journal of Global Optimization*, Vol. 18, December 2000, pp. 367–383.

[27] A. Cassioli, D. Izzo, D. Di Lorenzo, M. Locatelli, and F. Schoen, "Global Optimization Approaches for Optimal Trajectory Planning," *Modeling and Optimization in Space Engineering* (G. Fasano and J. D. Pintr, eds.), Vol. 73 of *Springer Optimization and Its Applications*, pp. 111–140, Springer New York, 2013.

[28] "NASA Launch Services Program Performance Web Site," October 2014.

[29] "SPICE Ephemeris," August 2013. `http://naif.jpl.nasa.gov/naif/`.

[30] J. A. Englander, B. A. Conway, and T. Williams, "Automated Interplanetary Mission Planning," *AAS/AIAA Astrodynamics Specialist Conference, Minneapolis, MN*, August 2012.

[31] V. Pareto, *Manuale di Economica Politica*. Milano, Italy: Societa Editrice Libraria, 1906. translated into English by A. Schwier as Manual of Political Economy, MacMillan Press, New York, 1971.

[32] C. A. Coello, G. B. Lamont, and D. A. Veldhuizen, *Evolutionary Algorithms for Solving Multi-Objective Problems (Genetic and Evolutionary Computation), 2nd ed.* Springer-Verlag, 2006.

[33] "MPI: A Message-Passing Interface Standard," tech. rep., Message Passing Forum, Knoxville, TN, USA, 1994.

[34] C. Yam, D. d. Lorenzo, and D. Izzo, "Low-Thrust Trajectory Design as a Constrained Global Optimization Problem," *Proceedings of the Institution of Mechanical Engineers, Part G: Journal of Aerospace Engineering*, Vol. 225, 2011, pp. 1243–1251.

[35] P. E. Gill, W. Murray, and M. A. Saunders, "SNOPT: An SQP Algorithm for Large-Scale Constrained Optimization," *SIAM Rev.*, Vol. 47, No. 1, 2005, pp. 99–131.

[36] "Deep Impact: Your First Look Inside a Comet!," `http://deepimpact.umd.edu/`.

[37] "Stardust-NExT," `http://stardustnext.jpl.nasa.gov/`.

[38] "JPL Small-Body Database Search Engine," June 1 2015.

[39] "EMTG (Evolutionary Mission Trajectory Generator)," `https://sourceforge.net/projects/emtg/`.